Multiaxial elastoplastic cyclic loading of austenitic 316L steel

V. Mazánová, J. Polák, V. Škorík, T. Kruml
Institute of Physics of Materials, Academy of Sciences of the Czech Republic
mazanova@ipm.cz
*polak@ipm.cz, http://orcid.org/*0000-0002-0457-4680
skorik@ipm.cz
*kruml@ipm.cz, http://orcid.org/*0000-0002-8855-1709

ABSTRACT. Cyclic stress-strain response and fatigue damage character has been investigated in austenitic stainless steel 316L. Hollow cylindrical specimens have been cyclically deformed in combined tension-compression and torsion under constant strain rate condition and different constant strain and shear strain amplitudes. In-phase and 90° out-of-phase cyclic straining was applied and the stress response has been monitored. Cyclic hardening/softening curves were assessed in both channels. Cyclic softening followed for higher strain amplitudes by long-term cyclic hardening was observed. Cyclic stress-strain curves were determined. Study of the surface damage in fractured specimens revealed the types and directions of principal cracks and the sources of fatigue crack initiation in slip bands.

KEYWORDS. Multiaxial cyclic loading; 316L steel; Cyclic stress-strain curve; Crack initiation.

Citation: Mazánová, V., Polák, J., Škorík, V., Kruml, T., Multiaxial elastoplastic cyclic loading of austenitic 316L steel, Frattura ed Integrità Strutturale, 40 (2017) 162-169.

Received: 09.01.2016
Accepted: 10.02.2017
Published: 01.04.2017

INTRODUCTION

Cyclic plastic response and damage evolution in elastoplastic cyclic loading of stainless steels, specifically 316L steel, has been studied mostly in tension-compression (see e.g.[1, 2]) but also in torsion [3] and less frequently in multiaxial loading [4, 5]. Characteristic feature of cyclic plastic straining of 316L steel at room and depressed temperatures is the localization of the cyclic plastic strain. The localization of the cyclic strain into persistent slip bands (PSBs) influences its cyclic plastic response and results in formation of persistent slip markings (PSMs) in which fatigue cracks initiate.

The subject of the present contribution is to extend the study of the cyclic plastic response and early fatigue damage to tubular specimens of 316L austenitic steel subjected to cyclic tension-compression and torsion biaxial cyclic loading. Simultaneously the early stages of the fatigue damage in the form of PSMs and initiation of fatigue cracks under in-phase and 90°out-of phase straining are reported.

EXPERIMENTAL

The material studied was commercial AISI 316L stainless steel supplied by Thyssen in the form of a round bar of 20 mm in diameter. Its chemical composition (in wt.%) was as follows: 0.017 C, 1.60 Mn, 0.497 Si, 0.029 P, 0.027 S, 16.70 Cr, 10.1 Ni, 2.03 Mo, 0.031 Ca and 0.078 N. The bar was hot rolled; $\sigma_{0.2}$ = 295 MPa. The microstructure was formed by equiaxed austenite grains with the average austenite grain size was 80 μm and some delta ferrite bands. The hollow cylindrical specimens with dimensions shown in Fig. 1 were machined from the round bars. No heat treatment was applied after the machining.

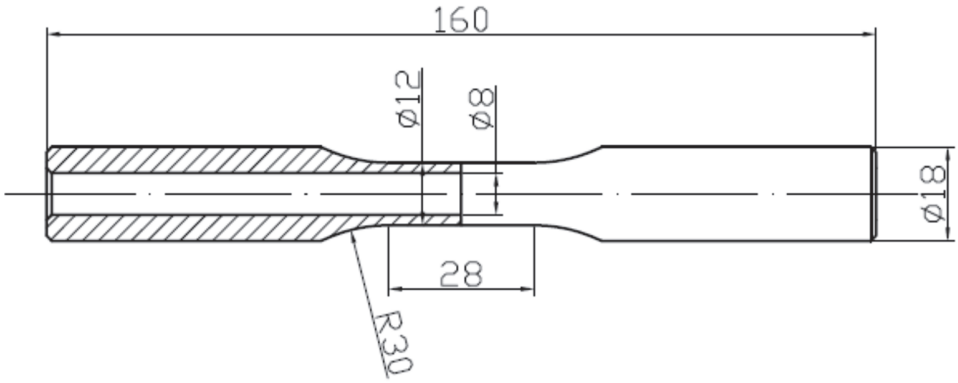

Figure 1: Geometry of the hollow cylindrical specimen

The gauge section was mechanically and electrolytically polished in order to achieve perfect surface for observation of the surface relief. All tests were performed in an electrohydraulic axial–torsion computer controlled MTS testing system. Combined axial-torsion extensometer was used to measure and control axial and shear strain. The tests were conducted under fully-reversed straining (R = -1) both in tension-compression and in torsion with constant strain rate. Axial strain rate was $5x10^{-3}$ s^{-1} and the shear strain rate on the specimen surface was equivalent to the axial strain rate. The strain in the middle diameter of the specimen is reported. Plastic strain was evaluated by subtracting the elastic component from the total strain.

Since the fatigue behaviour of the material has been already thoroughly studied in axial testing [1, 6, 7] we have performed torsion tests and in phase and 90° out-of-phase biaxial tension-compression-torsion tests. The biaxial tests are reported here.

Surface relief and fatigue crack initiation was studied on cracked specimens using optical microscope, SEM observations and FIB cutting. The surface of the specimen was inspected in FEG-SEM Lyra 3 XMU (TESCAN) equipped with focused ion beam (FIB). In order to protect the surface of the fatigued specimen from the ions during the production of surface craters the area of observation containing the PSMs was first covered by the thin sheet of platinum using electron deposition and later thicker layer was applied using ion deposition. Sectioning using FIB was performed perpendicular to the surface and nearly perpendicular to the direction of PSMs. Final cutting was performed with small intensity to achieve smooth perpendicular surface. The cuts were imaged in secondary electrons under inclination of about 35 degrees. The effect of inclination was compensated in all images of the cuts.

RESULTS

Stress-strain response

Hysteresis loops were recorded during cycling in both channels (uniaxial and torsion). Fig. 2 shows typical shapes of hysteresis loops during in-phase cycling and 90° out-of-phase cycling. Appreciable softening is apparent in in-phase cycling. Much higher stress response has been registered in 90° out-of-phase cycling at approximately the same plastic strain amplitude. Specific shape of the hysteresis loop in 90°out-of phase straining is due to reversion of the strain rate direction in both channels.

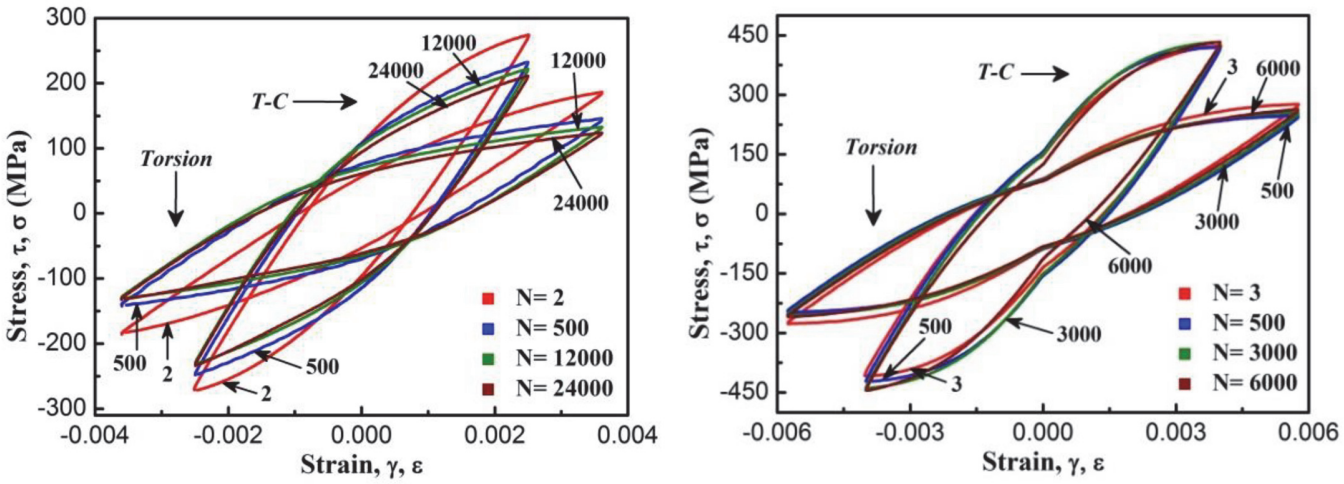

(a) (b)

Figure 2: Hysteresis loops in (a) in-phase cycling (b) 90° out-of-phase cycling.

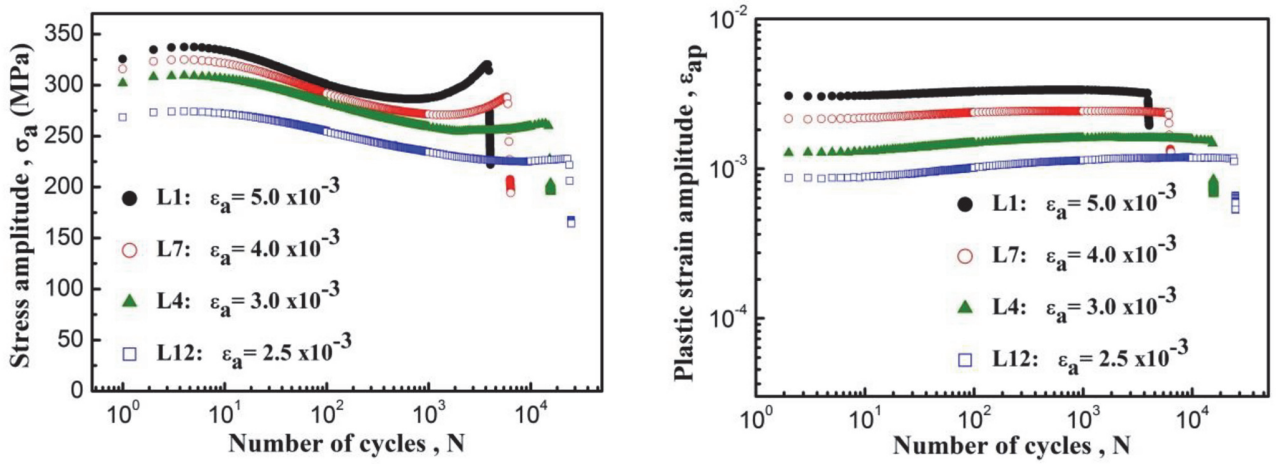

(a) (b)

Figure 3: Cyclic hardening/softening curves during in-phase cycling: (a) uniaxial stress amplitude vs. number of cycles, (b) plastic strain amplitude vs. number of cycles.

Figs 3 and 4 show in more detail the cyclic hardening and softening behavior. Except the very few initial cycles both tension-compression stress amplitude (Fig. 3a) and shear stress amplitude (Fig. 4a) decrease initially rapidly and either stabilize for the lowest strain amplitude or start to increase again towards the end of fatigue life.

During 90°out-of-phase cycling only small changes of the stress and plastic strain amplitude during fatigue life are found (Fig. 5). Early cyclic hardening is followed by mild softening for small strain amplitudes and hardening for high strain amplitudes both in tension-compression and in torsion. The level of the stress amplitude is considerably higher than in in-phase cycling.

The cyclic stress-strain curves have been plotted in Fig. 7 for in-phase and 90° out-of-phase cycling. The equivalent stress and plastic strain amplitudes in in-phase straining were calculated using von Misses relations

$$\sigma_{a,eq} = \sqrt{\left(\sigma_a^2 + 3\tau_a^2\right)} \tag{1}$$

$$\varepsilon_{a,eq} = \sqrt{\left(\varepsilon_a^2 + \frac{\gamma_a^2}{3}\right)} \tag{2}$$

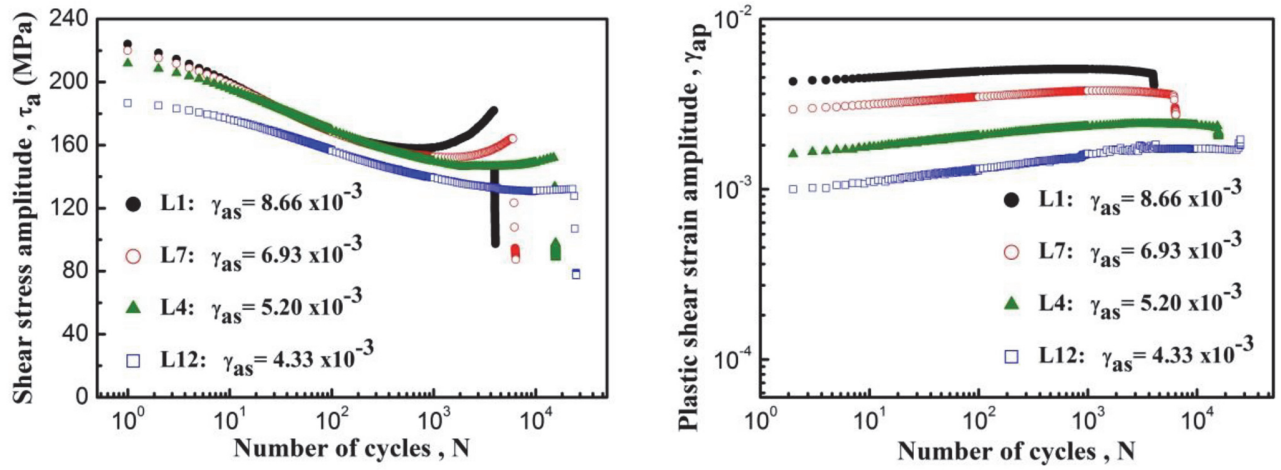

(a) (b)

Figure 4: Cyclic hardening/softening curves in in-phase cycling: (a) shear stress amplitude vs. number of cycles, (b) plastic shear strain amplitude vs. number of cycles.

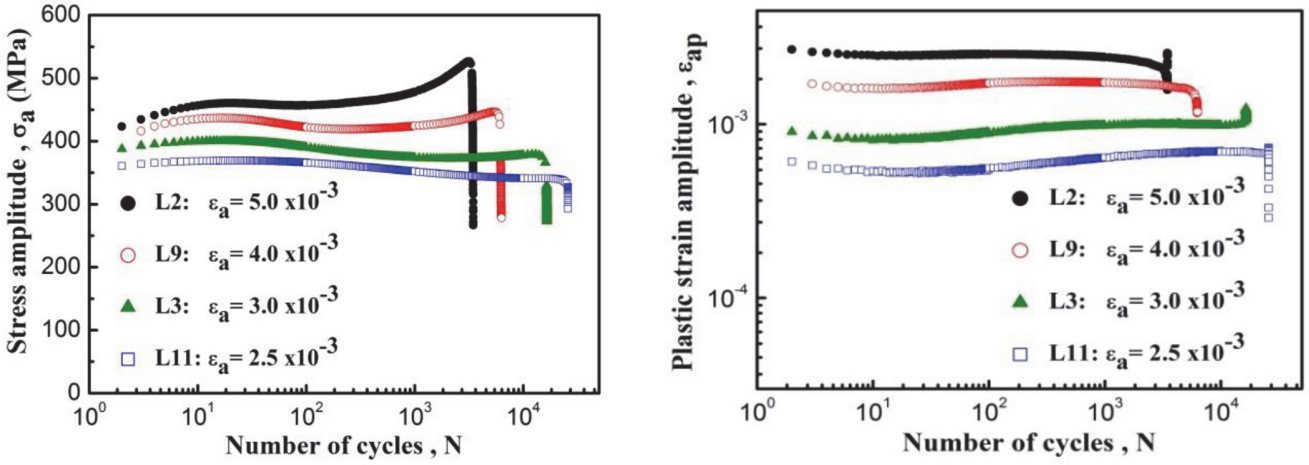

(a) (b)

Figure 5: Cyclic hardening/softening curves during 90°out-of-phase cycling: (a) uniaxial stress amplitude vs. number of cycles, (b) plastic strain amplitude vs. number of cycles.

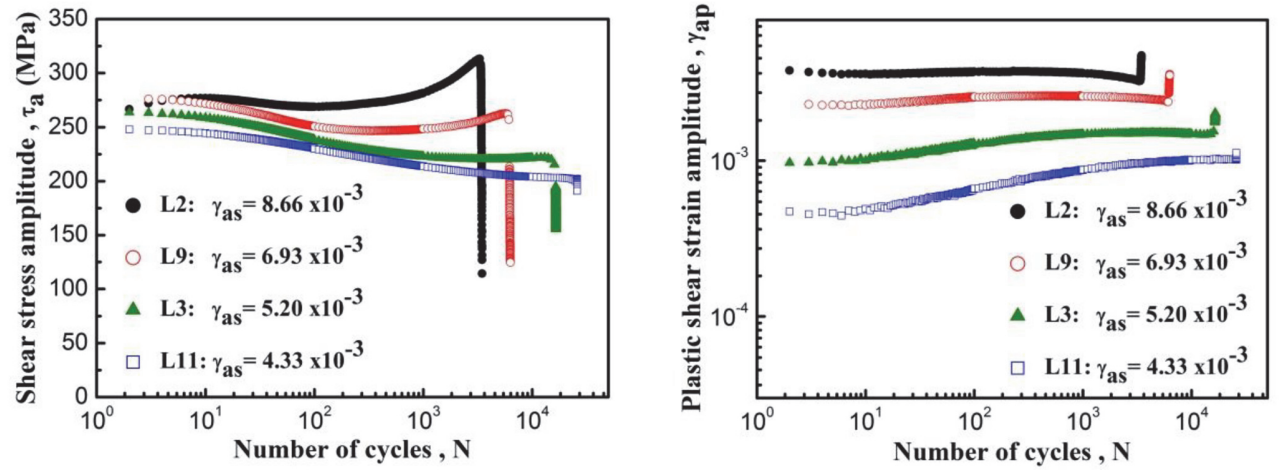

(a) (b)

Figure 6: Cyclic hardening/softening curves in 90°out-of-phase cycling: (a) shear stress amplitude vs. number of cycles, (b) plastic shear strain amplitude vs. number of cycles.

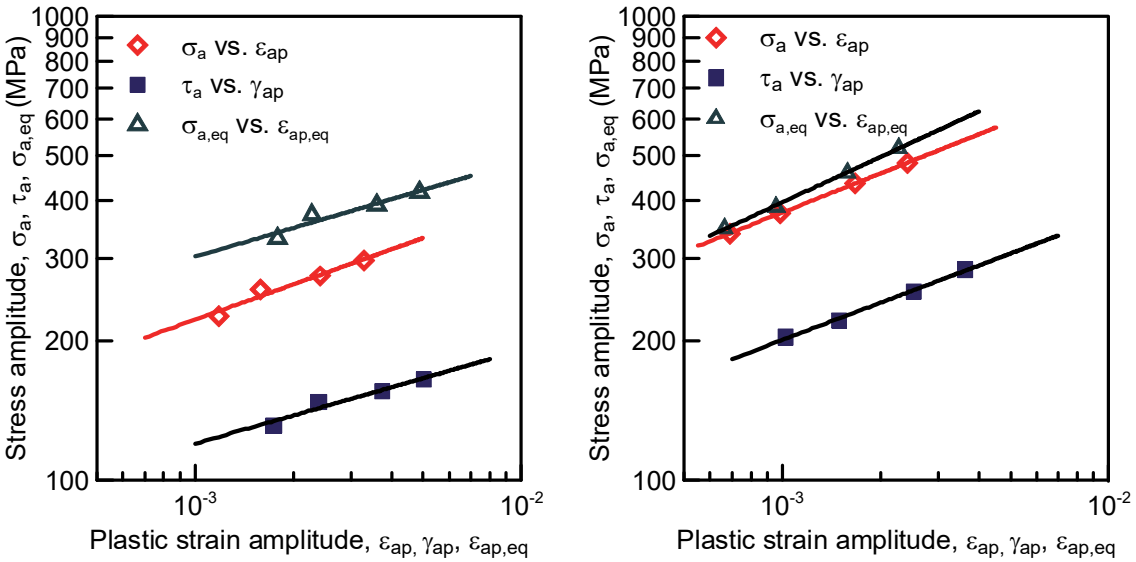

Figure 7: Cyclic stress-strain curves in biaxial cycling: (a) in-phase cycling, (b) out-of-phase cycling.

and equivalent plastic strain amplitude was evaluated using equation

$$\varepsilon_{a,eq,p} = \varepsilon_{a,eq} - \frac{\sigma_{a,eq}}{E_{eff}} \quad \sigma_a = K'\varepsilon_{ap}^{n'} \tag{3}$$

In 90° out-of-phase loading equivalent stress amplitude was evaluated using Eq. (1) but instead of using shear stress amplitude the shear stress corresponding to peak value of the axial stress was used. Equivalent strain amplitude was equal to the tension-compression strain amplitude. The effective modulus E_{eff} =190 GPa was used.
Cyclic stress-strain curve in equivalent stress and strain in in-phase straining lies above the cyclic stress-strain curve corresponding to tension-compression but has approximately the same slope. In 90°out-of-phase straining the cyclic stress-strain curve is only slightly above the cyclic stress-strain curve corresponding to tension-compression. All curves could be well approximated by the power law

$$\sigma_a = K'\varepsilon_{ap}^{n'} \tag{4}$$

The parameters of all cyclic stress-strain curves determined using least square fitting shows Tab. 1.

Type of loading	Tens.-comp. stress		Torsion stress		Equivalent stress	
	K′ (MPa)	n′	K′ (MPa)	n′	K′ (MPa)	n′
in-phase	1262	0.251	483	0.202	1258	0.206
90° out-of-phase	2604	0.279	1261	0.266	3758	0.325

Table 1: Parameters of the cyclic stress-strain curves

Early fatigue damage

Fractured specimens were studied in optical and scanning electron microscope. Multiple secondary cracks developed during the fatigue life in addition to the principal crack. The majority of larger cracks were inclined approximately 45 degrees to the specimen axis. The central part of one of these macroscopic cracks is shown in Fig. 8a. It is evident that the crack path is rugged since the crack microscopically often follows crystallographic planes.

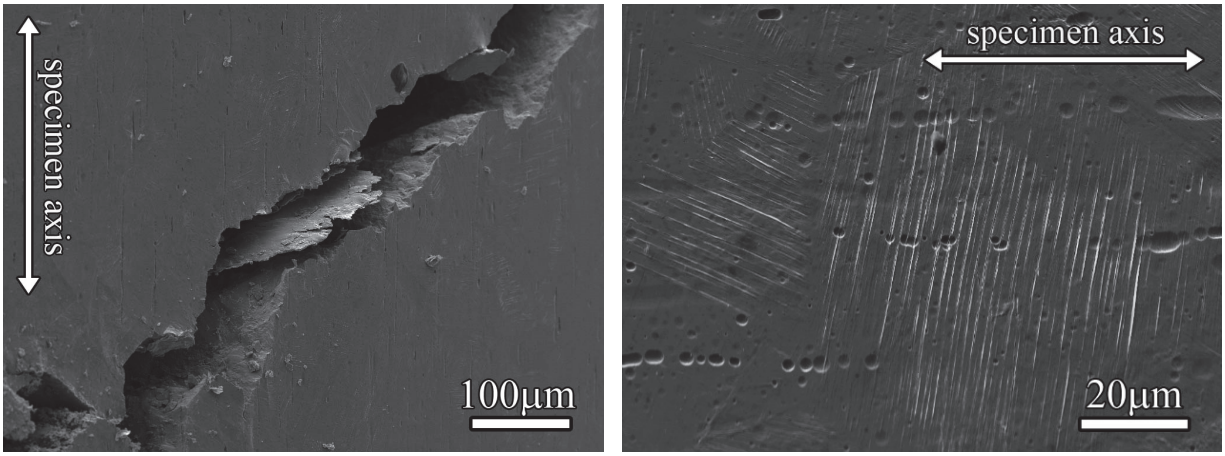

(a) (b)

Figure 8: Surface of the specimen cycled in-phase cyclic straining to fracture: (a) central part of the macroscopic crack, (b) parallel PSMs in surface grains.

We were interested in the early stages of the damage i.e. the initiation of the cracks. Fig. 8b shows the surface with grains covered by a system of PSMs. No clear crack is apparent from this picture. Also high resolution image did not allow to distinguish extrusions-intrusions and cracks. FIB cut performed on the area covered by a platinum layer reveals the shapes of extrusions and intrusions and the presence of a deep crack starting from one of the intrusions (Fig. 9a). Fig 9b shows the details of the surface relief in the location of the cut revealing several cracks starting from intrusions.

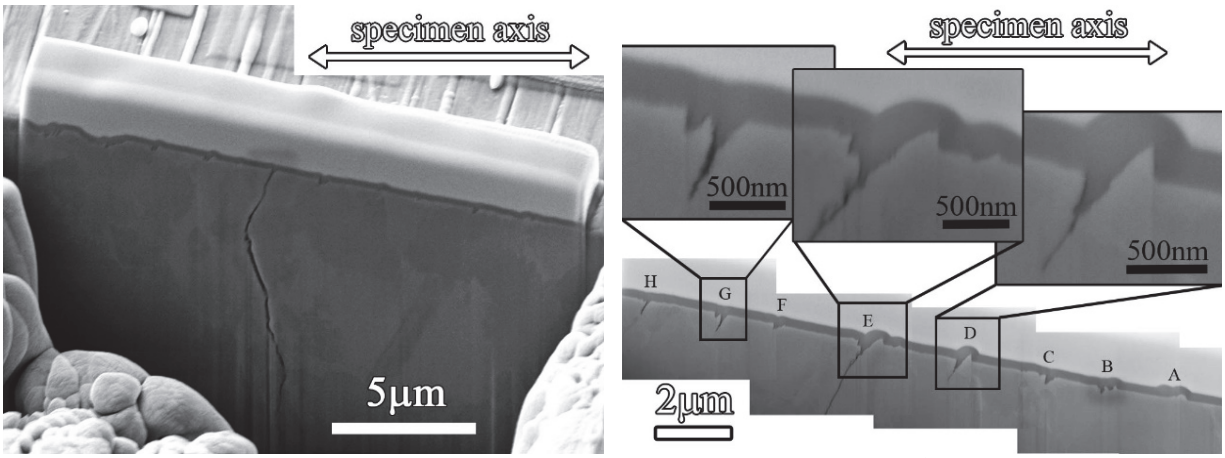

(a) (b)

Figure 9: Surface profile of PSMs produced by in-phase cycling: (a) FIB cut, (b) details of the surface profile.

Similar surface cracking and initiation of fatigue cracks was found in out-of-phase cyclic straining. Fig. 10a shows typical secondary crack and Fig. 10b the area with the PSMs. The image of the surface profile extracted from the FIB cut perpendicular to the direction of the PSMs is inserted in the picture. PSMs consist mostly of extrusions but PSMs B, E and F have also an intrusion which runs parallel to the extrusion.

Discussion

Cyclic plastic response of 316L steel in in-phase biaxial loading is close to that in uniaxial tension-compression loading [1, 6-8]. Cyclic hardening/softening curves which show long-term softening followed by cyclic hardening at higher strain amplitudes are nearly identical with those measured by Hong et al. [8] in tension-compression. Cyclic hardening/softening curves in 90° out-of-phase cycling are similar but are shifted to higher stress amplitudes.

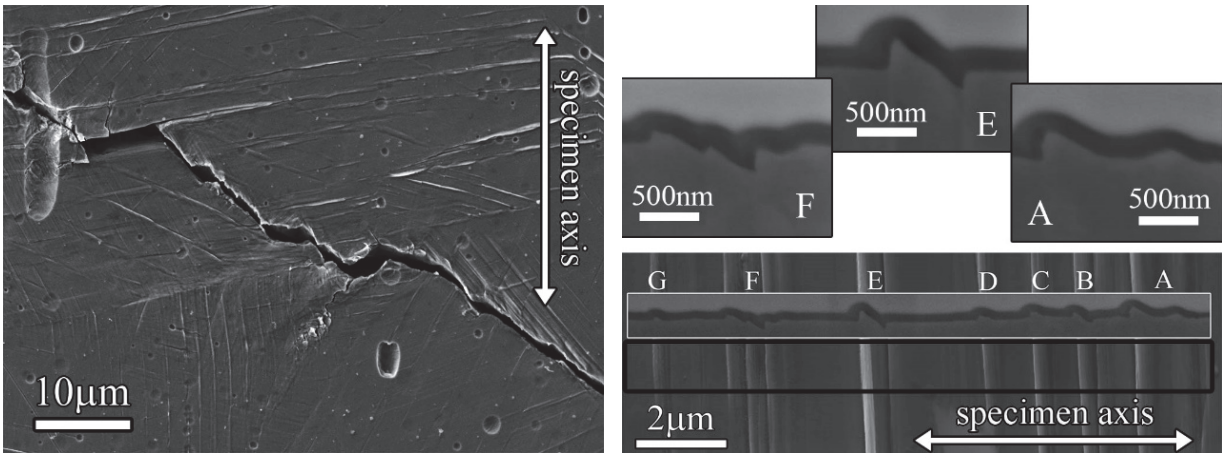

(a) (b)

Figure 10: Surface of the specimen cycled in 90°out-of phase straining to fracture: (a) central part of the secondary macroscopic crack, (b) PSMs in a grain and their profiles.

Cyclic stress-strain curves were plotted both for both individual channels and in equivalent stress and strain. Equivalent strain could be defined easily for in-phase straining. For 90° out-of-phase (diamond) straining the strain amplitude is reasonably well given by the tension-compression strain amplitude. However, the strain direction in a cycle changes and the strain path is more complicated. The cyclic stress-strain curve in equivalent stress and strain defined above lies above the cyclic stress-strain curves corresponding to tension-compression and torsion and has slightly higher slope.
Comparison of the equivalent cyclic stress-strain curves for in-phase and for 90° out-of-phase straining shows that due to the complicated strain path in 90° out-of-phase cycling the cyclic stress-strain curve is well above that of in in-phase straining. It is also apparent from Tab. 1 where the parameters of all cyclic stress-strain curves are listed.
The study of the surface of the specimens subjected to biaxial cyclic straining revealed general trend of the cracking in low cycle fatigue domain and also the early damage induced by in-phase and in 90° out-of-phase cycling. Macroscopic cracks grow at the angle around 45° to the specimen axis.
The initial stages of fatigue damage were studied in more detail. The study of the PSMs and small secondary cracks on the surface of the specimen revealed the profile of persistent slip markings consisting of extrusions and intrusions. Intrusions represent crack-like surface defect with high stress concentration factor. Fatigue cracks start from intrusions and grow along primary slip plane, usually on the boundary between the PSB and the matrix. This mechanism is the same as observed in uniaxial cyclic loading [2].

ACKNOWLEDGEMENT

The present work was conducted in the frame of IPMinfra supported through project No. LM2015069 and the project CEITEC 2020 No. LQ1601 of MEYS. The support by the project RVO: 68081723 and grants 13-23652S and 15-08826S of GACR is gratefully acknowledged.

REFERENCES

[1] Alain, R., Violan, P., Mendez, J., Low cycle fatigue behavior in vacuum of a 316L type austenitic stainless steel between 20 and 600 degrees C .1. Fatigue resistance and cyclic behavior, Mater. Sci. Eng., A 229 (1997) 87-94
[2] Man, J., Valtr, M., Petrenec, M., et al., AFM and SEM-FEG study on fundamental mechanisms leading to fatigue crack initiation, Int. J. Fatigue, 76 (2015) 11-18; DOI 10.1016/j.ijfatigue.2014.09.019.
[3] Wang, Y., Kimura, H., Akiniva, Y., et al., EBSD-AFM Hybrid analysis of crack initiation in stainless steel under fatigue loading, Key Eng. Mater., 340-341 (2007) 531-536.
[4] Jacquelin, B., Hourlier, F., Pineau, A., Crack Initiation under Low-Cycle Multiaxial Fatigue in Type-316l Stainless-Steel, J. Press. Vess.-T. ASME, 105 (1983) 138-143.

[5] Shamsaei, N., Fatemi, A., Socie, D.F., Multiaxial fatigue evaluation using discriminating strain paths, Int. J. Fatigue, 33 (2011) 597-609; 10.1016/j.ijfatigue.2010.11.002.
[6] Polák, J., Obrtlik, K., Hajek, M., Cyclic Plasticity in Type 316L Austenitic Stainless-Steel, Fatigue Fract. Eng. Mater., 17 (1994) 773-782.
[7] Pham, M.S., Holdsworth, S.R., Janssens, K.G.F., Mazza, E., Dislocation structure evolution and its effects on cyclic deformation response of AISI 316L stainless steel, Mater. Sci. Eng. A, 528 (2011) 3261-3269; 10.1016/j.msea.2011.01.015.
[8] Hong, S.G., Lee, S.B., Byun, T.S., Temperature effect on the low-cycle fatigue behavior of type 316L stainless steel: Cyclic non-stabilization and an invariable fatigue parameter, Mater. Sci. Eng. A, 457 (2007) 139-147; 10.1016/j.msea.2006.12.035.